Electronic Supplementary Material (ESI) for Journal of Materials Chemistry C.

Electronic Supplementary Information for

White light emission with unit efficiency from $Cs_2Na_{1-x}Ag_xIn_{1-y}Bi_yCl_6$ double perovskites: the role of bismuth and silver

Fang Liu,[a] Angelica Simbula,[a] Stefano Lai,[a] Luyan Wu,[a] Qingqian Wang,[b] Daniela Marongiu*[a] Riccardo Pau,[a,c] Selene Matta,[a] Federico Pitzalis,[a] Alessandra Geddo Lehmann,[a] Kai Wang,[b] Alessio Filippetti,[a,d] Francesco Quochi*[a] Michele Saba,[a] Andrea Mura,[a] Giovanni Bongiovanni[a]

[a] *Dipartimento di Fisica, Università degli Studi di Cagliari, Monserrato (CA), I-09042, Italy. E-mail: daniela.marongiu@dsf.unica.it, quochi@unica.it*

[b] *Department of Electrical and Electronic Engineering, Southern University of Science and Technology, Shenzhen, 518055, China*

[c] *Zernike Institute for Advanced Materials, University of Groningen, Nijenborgh 4, 09747 AG Groningen, The Netherlands*

[d] *Istituto Officina dei Materiali (CNR - IOM) Cagliari, Monserrato (CA), I-09042, Italy*

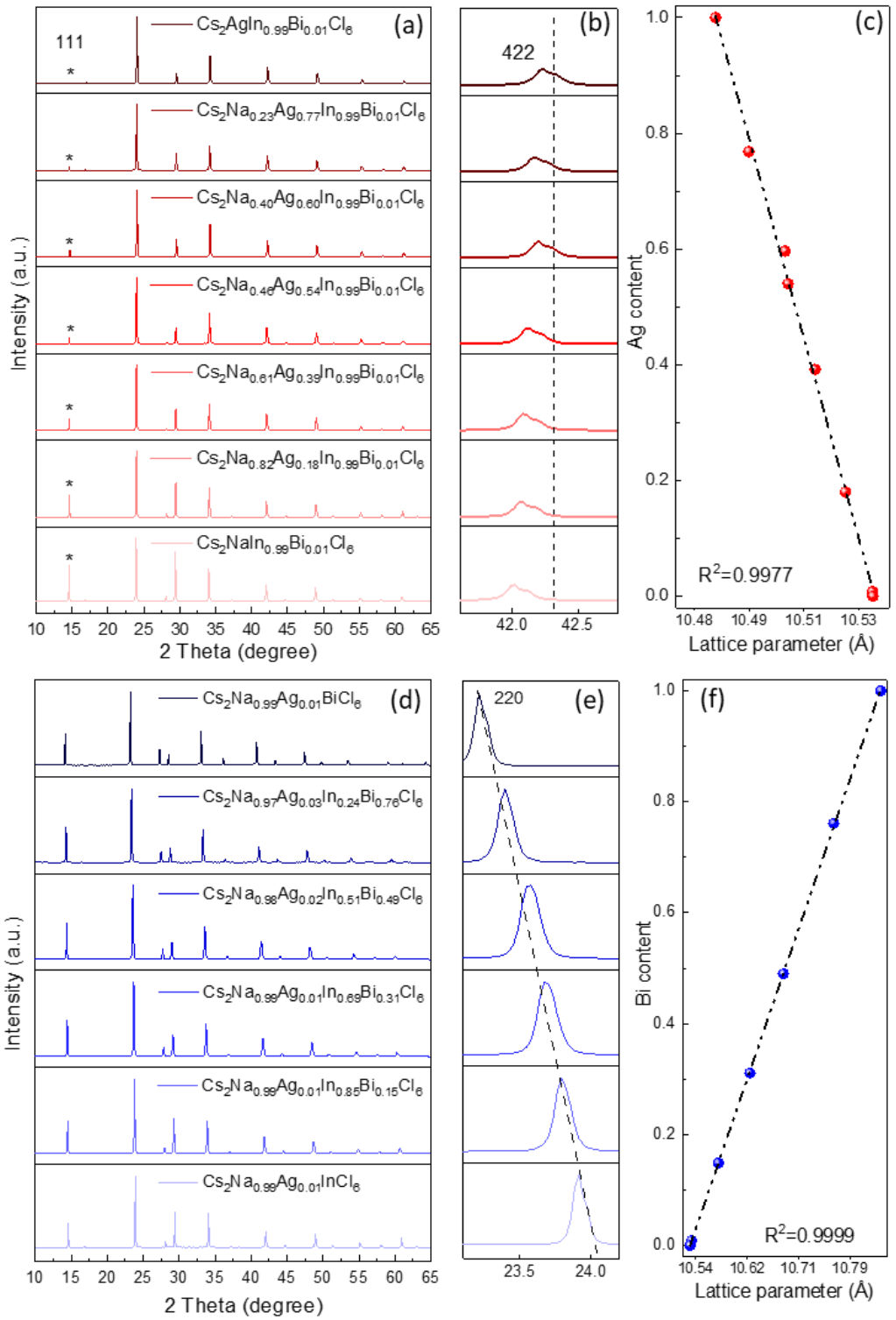

Fig. S1 (a) PXRD patterns of $Cs_2Na_{1-x}Ag_xIn_{0.99}Bi_{0.01}Cl_6$ with different Na/Ag ratio. (b) Enlarged view of (422) diffraction peak shift. (c) The cubic crystal lattice parameter as a function of Ag content. (d) PXRD patterns of $Cs_2Na_{0.99}Ag_{0.01}In_{1-y}Bi_yCl_6$ with different In/Bi ratio. (e) Enlarged view of (220) diffraction peak shift. (f) The cubic crystal lattice parameter as a function of Bi content.

Table S1 Inductively coupled plasma optical emission spectrometer (ICP-OES) results and lattice parameter of $Cs_2Na_{1-x}Ag_xIn_{1-y}Bi_yCl_6$.

Nominal composition	ICP-OES results	Refined lattice parameter (Å)
$Cs_2Na_{1-x}Ag_xInCl6$ & $Cs_2Na_{1-x}Ag_xIn_{0.99}Bi_{0.01}Cl_6$		
$Cs_2AgInCl_6$	$Cs_2AgInCl_6$	10.4787
$Cs_2Na_{0.2}Ag_{0.8}InCl_6$	$Cs_2Na_{0.22}Ag_{0.78}InCl_6$	10.4898
$Cs_2Na_{0.4}Ag_{0.6}InCl_6$	$Cs_2Na_{0.44}Ag_{0.56}InCl_6$	10.5019
$Cs_2Na_{0.5}Ag_{0.5}InCl_6$	$Cs_2Na_{0.51}Ag_{0.49}InCl_6$	10.5073
$Cs_2Na_{0.6}Ag_{0.4}InCl_6$	$Cs_2Na_{0.60}Ag_{0.40}InCl_6$	10.5096
$Cs_2Na_{0.8}Ag_{0.2}InCl_6$	$Cs_2Na_{0.85}Ag_{0.15}InCl_6$	10.5236
$Cs_2NaInCl_6$	$Cs_2NaInCl_6$	10.5325
$Cs_2AgIn_{0.99}Bi_{0.01}Cl6$	$Cs_2AgIn_{0.99}Bi_{0.01}Cl_6$	10.4830
$Cs_2Na_{0.2}Ag_{0.8}In_{0.99}Bi_{0.01}Cl6$	$Cs_2Na_{0.23}Ag_{0.77}In_{0.99}Bi_{0.01}Cl_6$	10.4939
$Cs_2Na_{0.4}Ag_{0.6}In_{0.99}Bi_{0.01}Cl6$	$Cs_2Na_{0.40}Ag_{0.60}In_{0.99}Bi_{0.01}Cl_6$	10.5059
$Cs_2Na_{0.5}Ag_{0.5}In_{0.99}Bi_{0.01}Cl6$	$Cs_2Na_{0.46}Ag_{0.54}In_{0.99}Bi_{0.01}Cl_6$	10.5068
$Cs_2Na_{0.6}Ag_{0.4}In_{0.99}Bi_{0.01}Cl6$	$Cs_2Na_{0.61}Ag_{0.39}In_{0.99}Bi_{0.01}Cl_6$	10.5157
$Cs_2Na_{0.8}Ag_{0.2}In_{0.99}Bi_{0.01}Cl6$	$Cs_2Na_{0.82}Ag_{0.18}In_{0.99}Bi_{0.01}Cl_6$	10.5256
$Cs_2Na_{0.99}Ag_{0.01}In_{0.99}Bi_{0.01}Cl6$	$Cs_2Na_{0.99}Ag_{0.01}In_{0.99}Bi_{0.01}Cl_6$	10.5346
$Cs_2NaIn_{0.99}Bi_{0.01}Cl6$	$Cs_2NaIn_{0.99}Bi_{0.01}Cl_6$	10.5347
$Cs_2NaIn_{1-y}Bi_yCl_6$ & $Cs_2Na_{0.99}Ag_{0.01}In_{1-y}Bi_yCl_6$		
$Cs_2NaBiCl_6$	$Cs_2NaBiCl_6$	
$Cs_2NaIn_{0.2}Bi_{0.8}Cl_6$	$Cs_2NaIn_{0.25}Bi_{0.75}Cl_6$	10.7652
$Cs_2NaIn_{0.4}Bi_{0.6}Cl_6$	$Cs_2NaIn_{0.49}Bi_{0.51}Cl_6$	10.6931
$Cs_2NaIn_{0.6}Bi_{0.4}Cl_6$	$Cs_2NaIn_{0.70}Bi_{0.30}Cl_6$	10.6269
$Cs_2NaIn_{0.8}Bi_{0.2}Cl_6$	$Cs_2NaIn_{0.85}Bi_{0.15}Cl_6$	10.5801
$Cs_2Na_{0.99}Ag_{0.01}BiCl_6$	$Cs_2Na_{0.99}Ag_{0.01}BiCl_6$	10.8398
$Cs_2Na_{0.99}Ag_{0.01}In_{0.2}Bi_{0.8}Cl_6$	$Cs_2Na_{0.97}Ag_{0.03}In_{0.24}Bi_{0.76}Cl6$	10.7639
$Cs_2Na_{0.99}Ag_{0.01}In_{0.4}Bi_{0.6}Cl_6$	$Cs_2Na_{0.98}Ag_{0.02}In_{0.51}Bi_{0.49}Cl6$	10.6829
$Cs_2Na_{0.99}Ag_{0.01}In_{0.6}Bi_{0.4}Cl_6$	$Cs_2Na_{0.99}Ag_{0.01}In_{0.69}Bi_{0.31}Cl_6$	10.6288
$Cs_2Na_{0.99}Ag_{0.01}In_{0.8}Bi_{0.2}Cl_6$	$Cs_2Na_{0.99}Ag_{0.01}In_{0.85}Bi_{0.15}Cl_6$	10.5780
$Cs_2Na_{0.99}Ag_{0.01}InCl_6$	$Cs_2Na_{0.99}Ag_{0.01}InCl_6$	10.5324

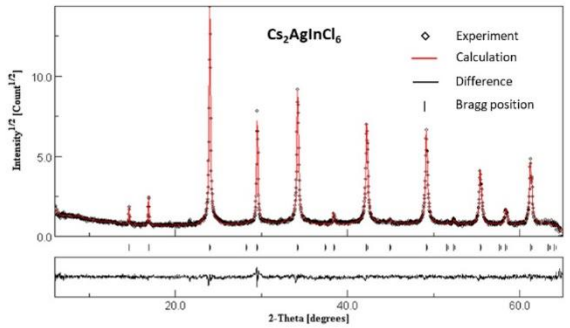
$Cs_2AgInCl_6$
Experiment
Calculation
Difference
Bragg position
Intensity$^{1/2}$ [Count$^{1/2}$]
2-Theta [degrees]

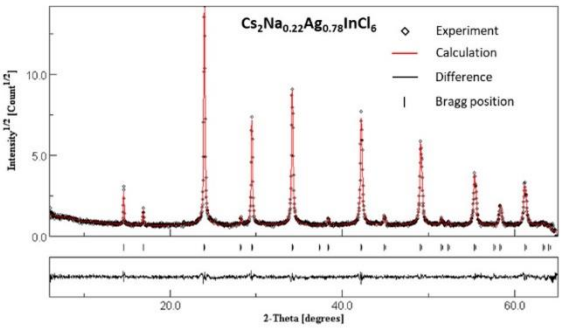
$Cs_2Na_{0.22}Ag_{0.78}InCl_6$
Experiment
Calculation
Difference
Bragg position
Intensity$^{1/2}$ [Count$^{1/2}$]
2-Theta [degrees]

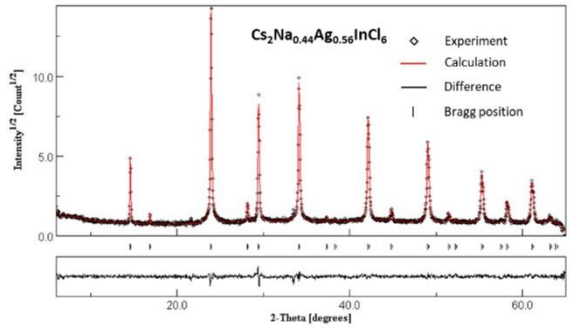
$Cs_2Na_{0.44}Ag_{0.56}InCl_6$
Experiment
Calculation
Difference
Bragg position
Intensity$^{1/2}$ [Count$^{1/2}$]
2-Theta [degrees]

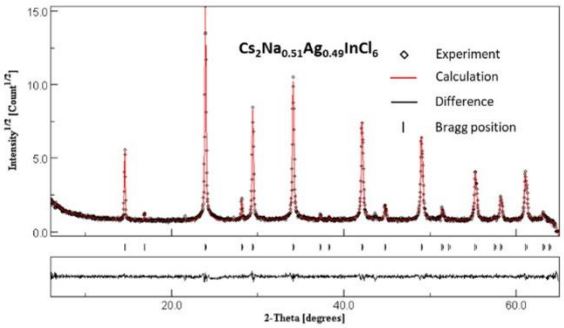
$Cs_2Na_{0.51}Ag_{0.49}InCl_6$
Experiment
Calculation
Difference
Bragg position
Intensity$^{1/2}$ [Count$^{1/2}$]
2-Theta [degrees]

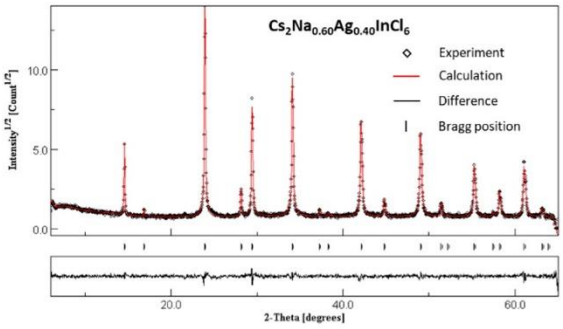
$Cs_2Na_{0.60}Ag_{0.40}InCl_6$
Experiment
Calculation
Difference
Bragg position
Intensity$^{1/2}$ [Count$^{1/2}$]
2-Theta [degrees]

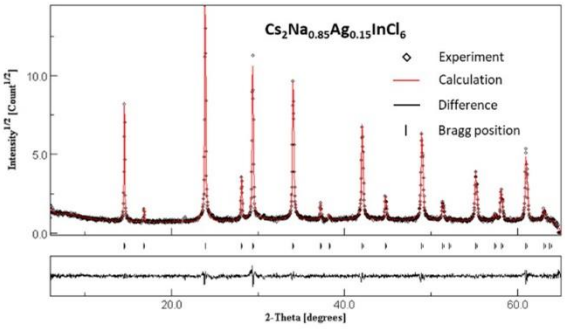
$Cs_2Na_{0.85}Ag_{0.15}InCl_6$
Experiment
Calculation
Difference
Bragg position
Intensity$^{1/2}$ [Count$^{1/2}$]
2-Theta [degrees]

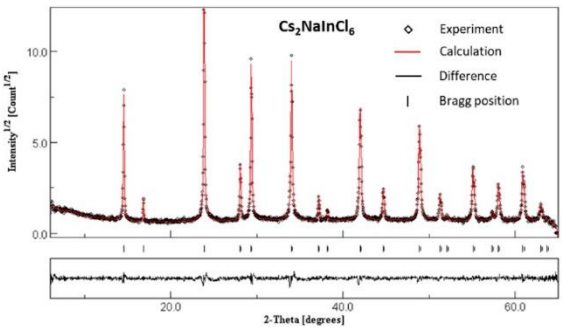
$Cs_2NaInCl_6$
Experiment
Calculation
Difference
Bragg position
Intensity$^{1/2}$ [Count$^{1/2}$]
2-Theta [degrees]

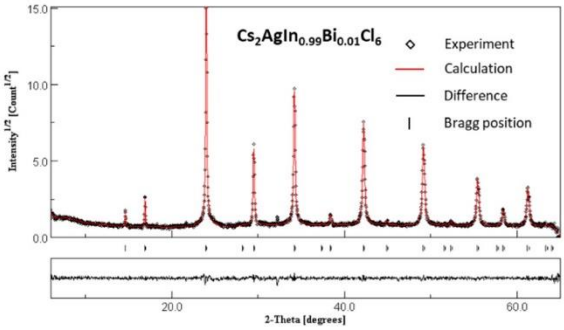
$Cs_2AgIn_{0.99}Bi_{0.01}Cl_6$
Experiment
Calculation
Difference
Bragg position
Intensity$^{1/2}$ [Count$^{1/2}$]
2-Theta [degrees]

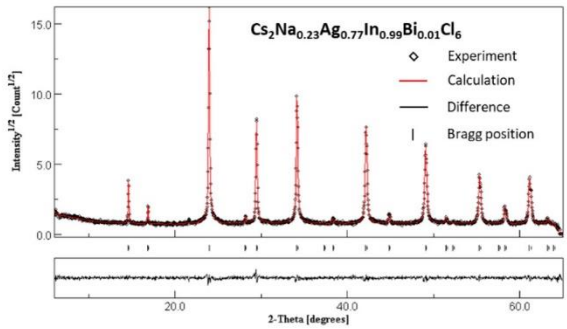
$Cs_2Na_{0.23}Ag_{0.77}In_{0.99}Bi_{0.01}Cl_6$
Experiment
Calculation
Difference
Bragg position
Intensity$^{1/2}$ [Count$^{1/2}$]
2-Theta [degrees]

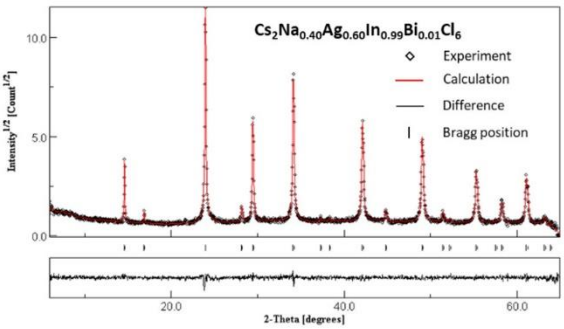
$Cs_2Na_{0.40}Ag_{0.60}In_{0.99}Bi_{0.01}Cl_6$
Experiment
Calculation
Difference
Bragg position
Intensity$^{1/2}$ [Count$^{1/2}$]
2-Theta [degrees]

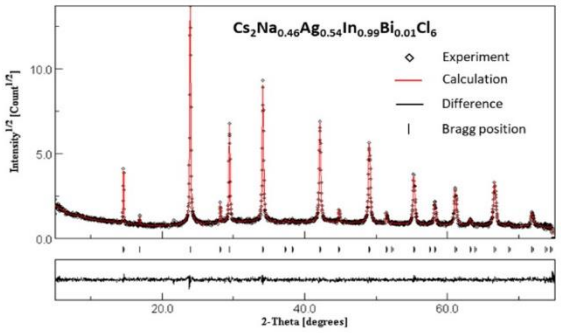
$Cs_2Na_{0.46}Ag_{0.54}In_{0.99}Bi_{0.01}Cl_6$
Experiment
Calculation
Difference
Bragg position
Intensity$^{1/2}$ [Count$^{1/2}$]
2-Theta [degrees]

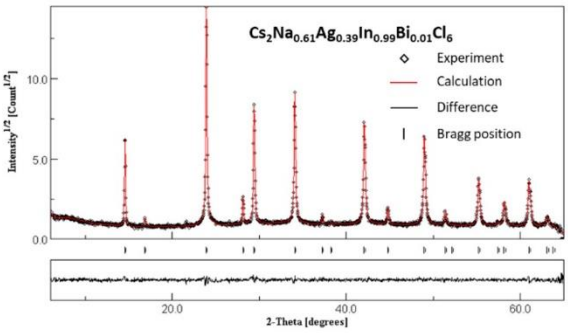
$Cs_2Na_{0.61}Ag_{0.39}In_{0.99}Bi_{0.01}Cl_6$
Experiment
Calculation
Difference
Bragg position
Intensity$^{1/2}$ [Count$^{1/2}$]
2-Theta [degrees]

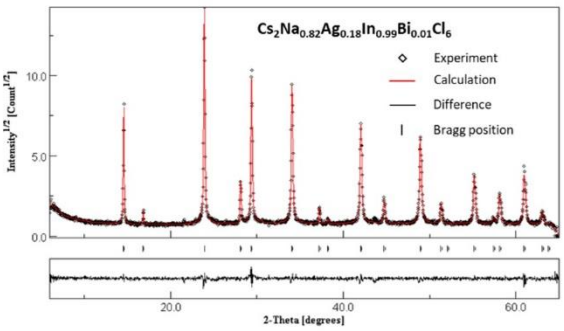
$Cs_2Na_{0.82}Ag_{0.18}In_{0.99}Bi_{0.01}Cl_6$
Experiment
Calculation
Difference
Bragg position
Intensity$^{1/2}$ [Count$^{1/2}$]
2-Theta [degrees]

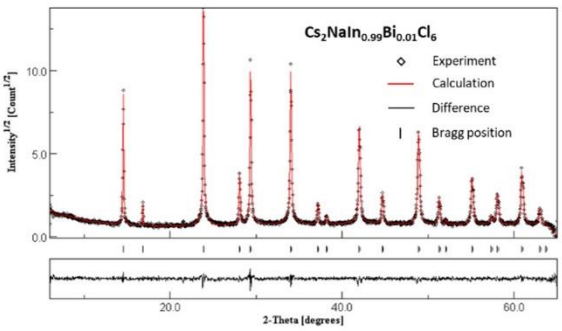
$Cs_2NaIn_{0.99}Bi_{0.01}Cl_6$
Experiment
Calculation
Difference
Bragg position
Intensity$^{1/2}$ [Count$^{1/2}$]
2-Theta [degrees]

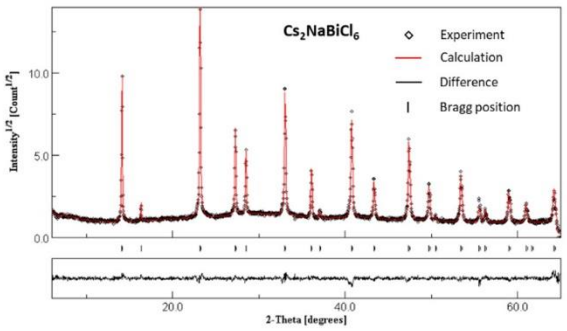
$Cs_2NaBiCl_6$
Experiment
Calculation
Difference
Bragg position
Intensity$^{1/2}$ [Count$^{1/2}$]
2-Theta [degrees]

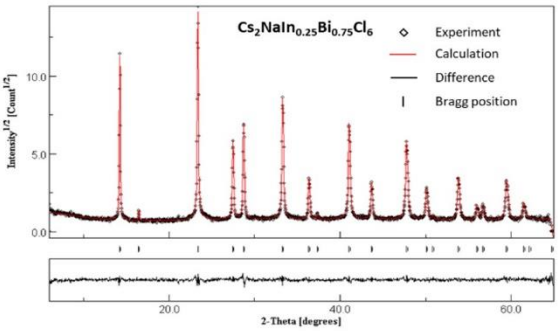
$Cs_2NaIn_{0.25}Bi_{0.75}Cl_6$
Experiment
Calculation
Difference
Bragg position
Intensity$^{1/2}$ [Count$^{1/2}$]
2-Theta [degrees]

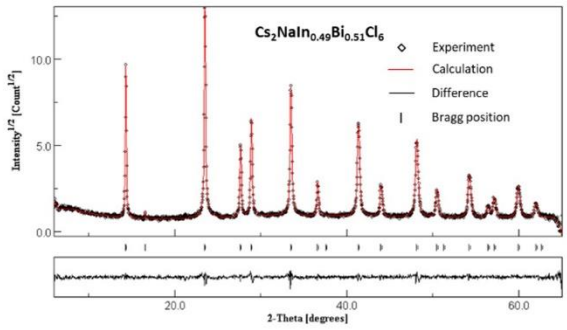
$Cs_2NaIn_{0.49}Bi_{0.51}Cl_6$
Experiment
Calculation
Difference
Bragg position
Intensity$^{1/2}$ [Count$^{1/2}$]
2-Theta [degrees]

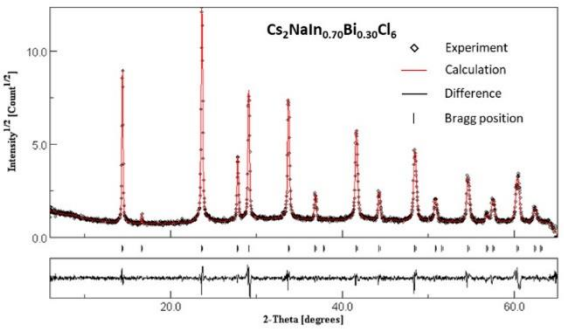
$Cs_2NaIn_{0.70}Bi_{0.30}Cl_6$
Experiment
Calculation
Difference
Bragg position
Intensity$^{1/2}$ [Count$^{1/2}$]
2-Theta [degrees]

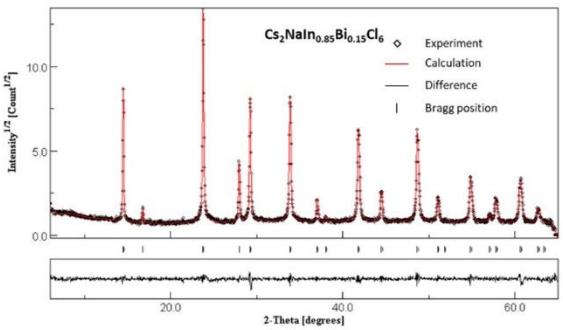
$Cs_2NaIn_{0.85}Bi_{0.15}Cl_6$
Experiment
Calculation
Difference
Bragg position
Intensity$^{1/2}$ [Count$^{1/2}$]
2-Theta [degrees]

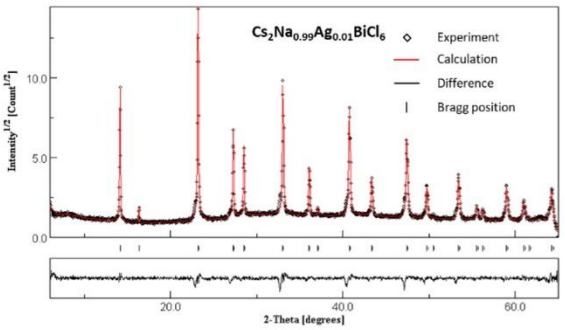
$Cs_2Na_{0.99}Ag_{0.01}BiCl_6$
Experiment
Calculation
Difference
Bragg position
Intensity$^{1/2}$ [Count$^{1/2}$]
2-Theta [degrees]

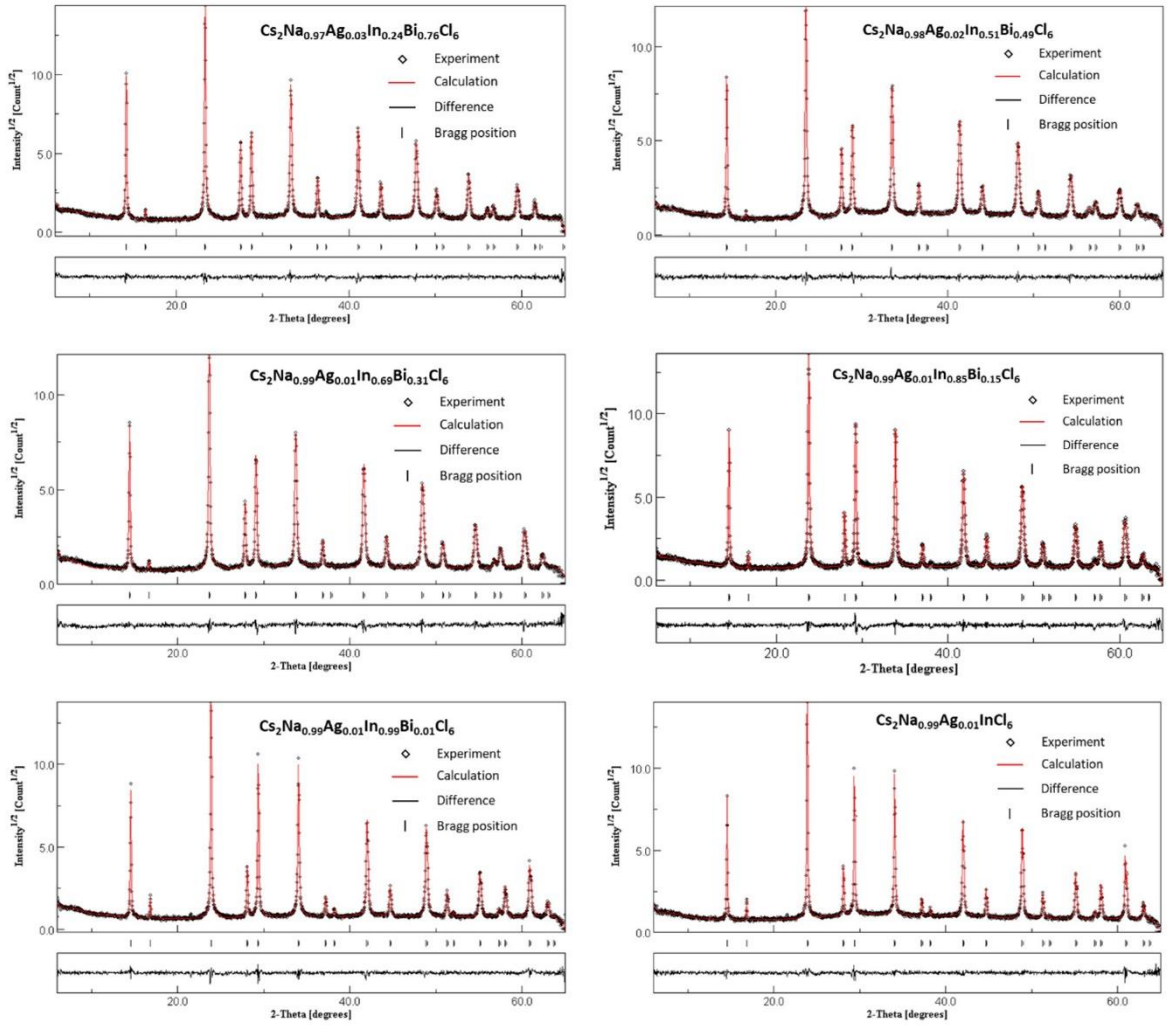

Fig. S2 Rietveld refinements of crystal samples $Cs_2AgIn_{1-y}Bi_yCl_6$, $Cs_2Na_{1-x}Ag_xInCl_6$, $Cs_2Na_{1-x}Ag_xIn_{0.99}Bi_{0.01}Cl_6$, $Cs_2NaIn_{1-y}Bi_yCl_6$, and $Cs_2Na_{0.99}Ag_{0.01}In_{1-y}Bi_yCl_6$. The lattice parameters are listed in Table S1.

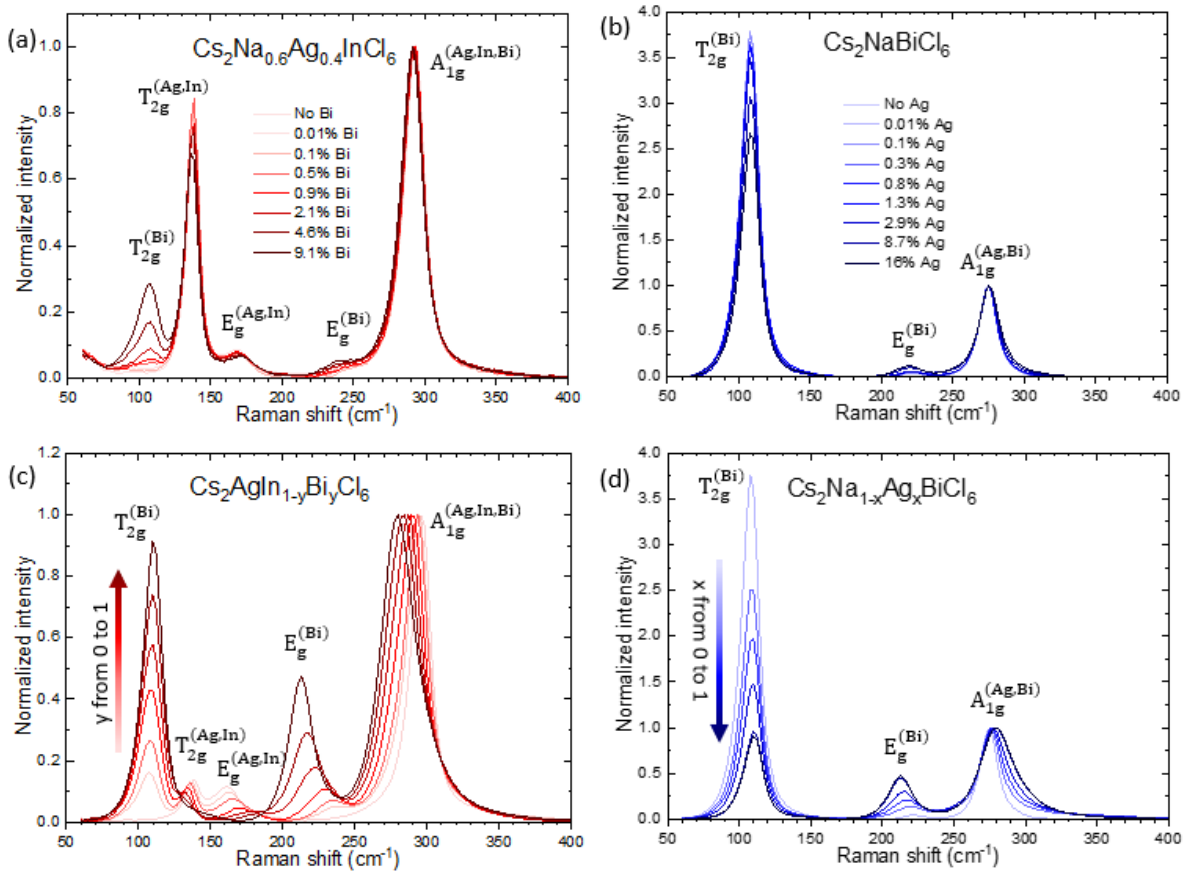

Fig. S3 Raman spectra of (a) $Cs_2Na_{0.6}Ag_{0.4}InCl_6$ alloyed with fraction of Bi from 0 to 9.1%, (b) $Cs_2NaBiCl_6$ alloyed with fraction of Ag from 0 to 16%, (c) $Cs_2AgInCl_6$ alloyed with fraction of Bi from 0 to 100% and (d) $Cs_2NaBiCl_6$ alloyed with fraction of Ag from 0 to 100%.

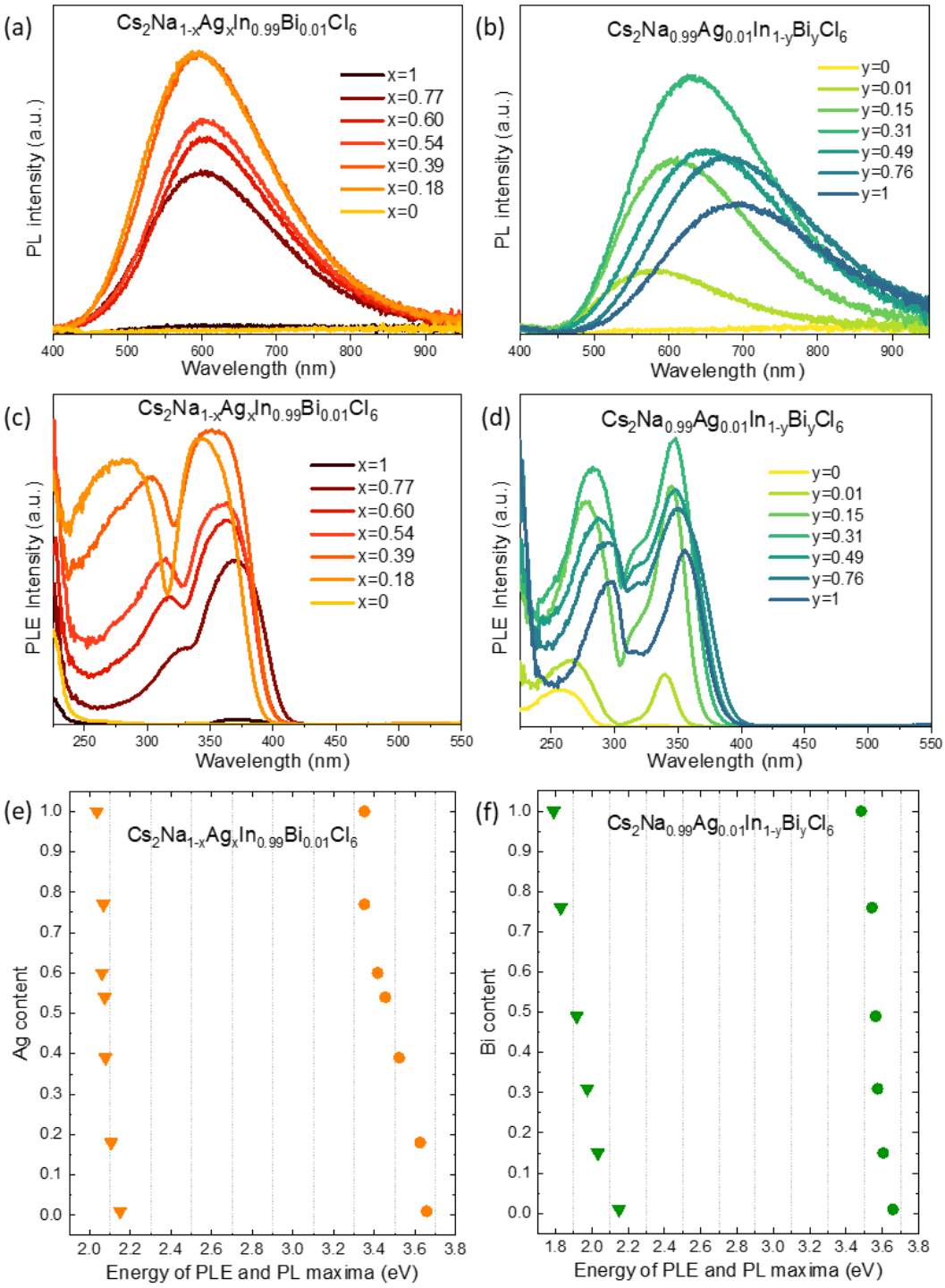

Fig. S4 PL (a) and PLE (c) spectra of $Cs_2Na_{1-x}Ag_xIn_{0.99}Bi_{0.01}Cl_6$ compounds; (b,d) Same as (a,c) but for $Cs_2Na_{0.99}Ag_{0.01}In_{1-y}Bi_yCl_6$ compounds. (e) PL (triangles) and PLE (circles) peak energies of $Cs_2Na_{1-x}Ag_xIn_{0.99}Bi_{0.01}Cl_6$ compounds; (f) Same as (e) but for $Cs_2Na_{0.99}Ag_{0.01}In_{1-y}Bi_yCl_6$ compounds.

Ab-initio calculations

In Fig. S5 we display the band structure of $Cs_2Na_{1-x}Ag_xIn_{1-y}Bi_yCl_6$ double perovskites for several *x* and *y* combinations, calculated by VPSIC. This overview highlights clearly the progressive band gap narrowing obtained for increasing Ag content; this is due to the combined effect of the Ag d valence bands and the shrinking of In s conduction bandwidth. In absence of In-Bi substitutions, all the compounds of the Na/Ag series suffer the parity-forbidden inter-band transition mechanism which largely suppresses the absorption rate at the band-gap edge, and shifts the optical absorption onset ~1 eV above in the energy. As discussed in the main text, this effect is substantially relieved even by a small fraction of In/Bi substitution.

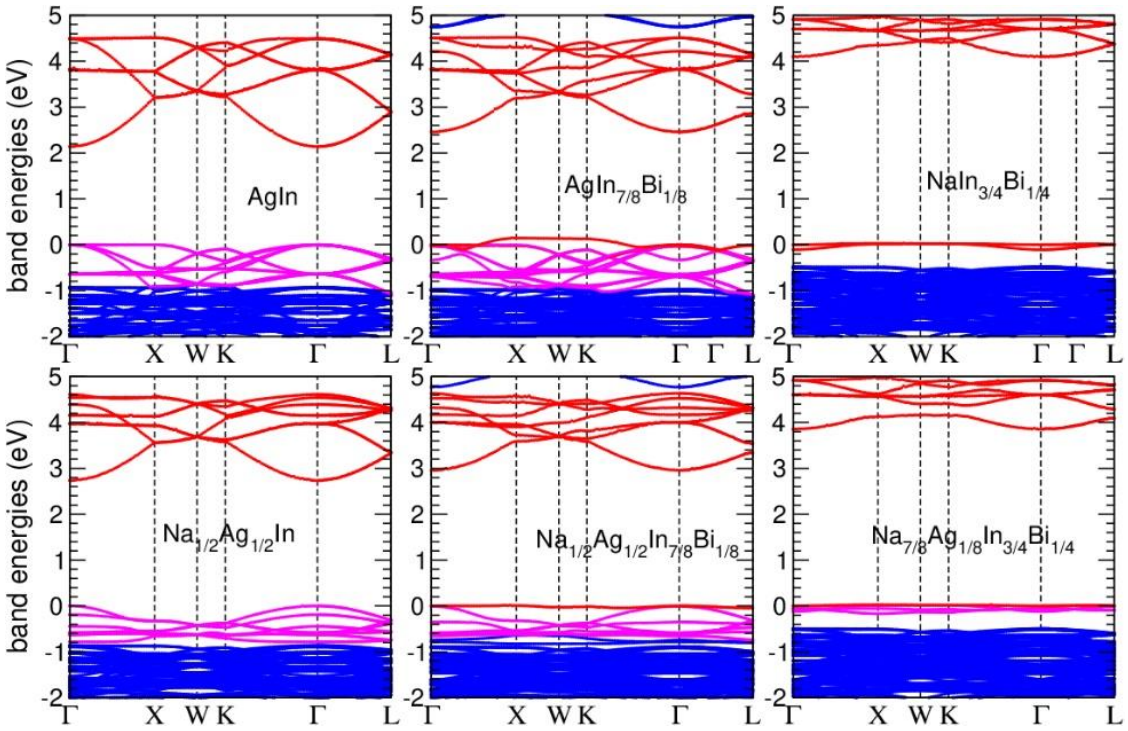

Fig. S5 VPSIC band energies calculated for various $Cs_2Na_{1-x}Ag_xIn_{1-y}Bi_yCl_6$ double perovskites; color code: red for conduction In s and valence Bi s bands; magenta for Ag 4d e.g., bands, blue for Cl p and Bi p bands.

In Fig. S6 we illustrate the effect of 25% In/Bi doping in pure Na compounds ($Cs_2NaIn_{3/4}Bi_{1/4}Cl_6$) and in 12.5% mixed Na/Ag compounds ($Cs_2Na_{7/8}Ag_{1/8}In_{3/4}Bi_{1/4}Cl_6$), in order to rationalize the combined action of Ag and Bi doping. We can see that both Bi and Ag introduce fairly localized electronic states at the valence band top, specifically Bi 6s and Ag e_g states, the latter visibly hybridized with Cl p ligands, as shown in the DOS. The strong localization of Bi 6s and Ag e_g states for 25% and 12.5% concentrations, respectively, is remarkable. The reason is related to the lack of hopping with nearest-neighbor Na and In states in the energy region near the VBT.

In fact, the Na DOS is not reported in figure since discardable in this energy range. The simultaneous presence of Bi and Ag apparently does not change significantly the absorption rate of the pure-Na compound at the band gap onset: in Fig. S6 we show that the absorption rate difference between the two materials is substantially related to the band gap offset, at least up to 0.5 eV above the band gap; in the 0.5-1.0 eV window, on the other hand, the presence of Ag is effective in increasing considerably the absorption rate. This is the region where the Ag t_{2g} states set in, thus giving a substantial contribution to the DOS with respect to the pure Na compound.

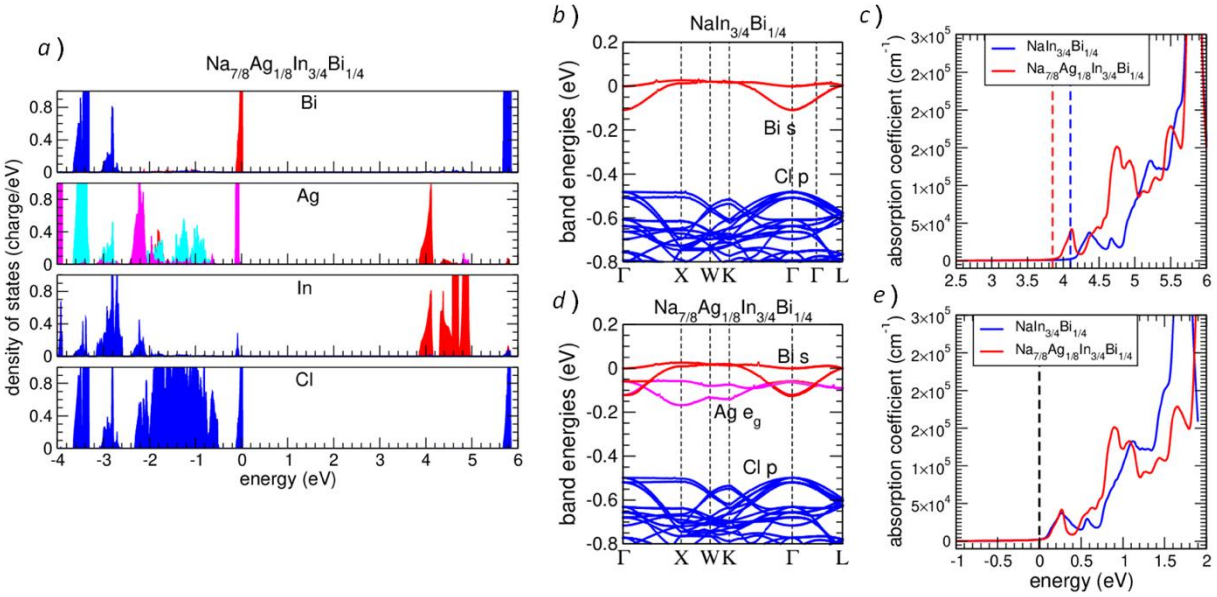

Fig. S6 VPSIC calculations for $Cs_2NaIn_{3/4}Bi_{1/4}Cl_6$ and $Cs_2Na_{7/8}Ag_{1/8}In_{3/4}Bi_{1/4}Cl_6$. a) Orbital-resolved DOS for $Cs_2Na_{7/8}Ag_{1/8}In_{3/4}Bi_{1/4}Cl_6$. Color code: s (red), p (blue), e_g (magenta), t_{2g} (cyan). b) band energies in a narrow window near the VBT for the two examined compounds; band colors correspond to those used for the DOS. c) absorption spectrum for the two compounds; the vertical dashed lines indicate the band gaps. In the lower panel, the two curves are shifted by the respective band gaps.

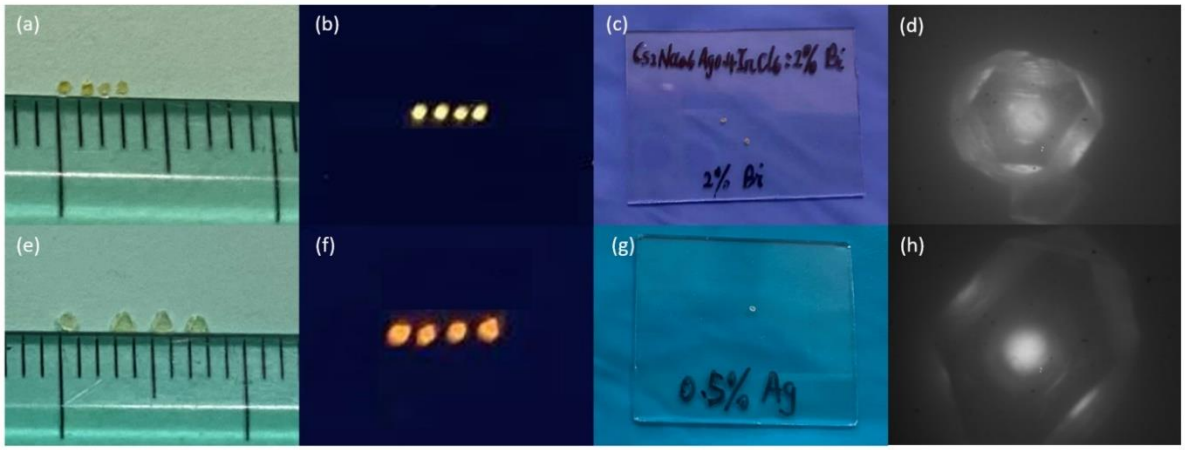

Fig. S7 The top row represents the alloyed double perovskite $Cs_2Na_{0.6}Ag_{0.4}In_{0.98}Bi_{0.02}Cl_6$ (nominal feeding ratio): Photos of single crystals (a) under day light, (b) under 365 nm UV light, (c) fixed on glass for tandem spectroscopy measurements; (d) PL image of single crystal photoexcited by the laser during tandem spectroscopy measurements. The bottom row represents the alloyed double perovskite $Cs_2Na_{0.995}Ag_{0.005}BiCl_6$ (nominal feeding ratio); (e-h) Same conditions as for (a-d).

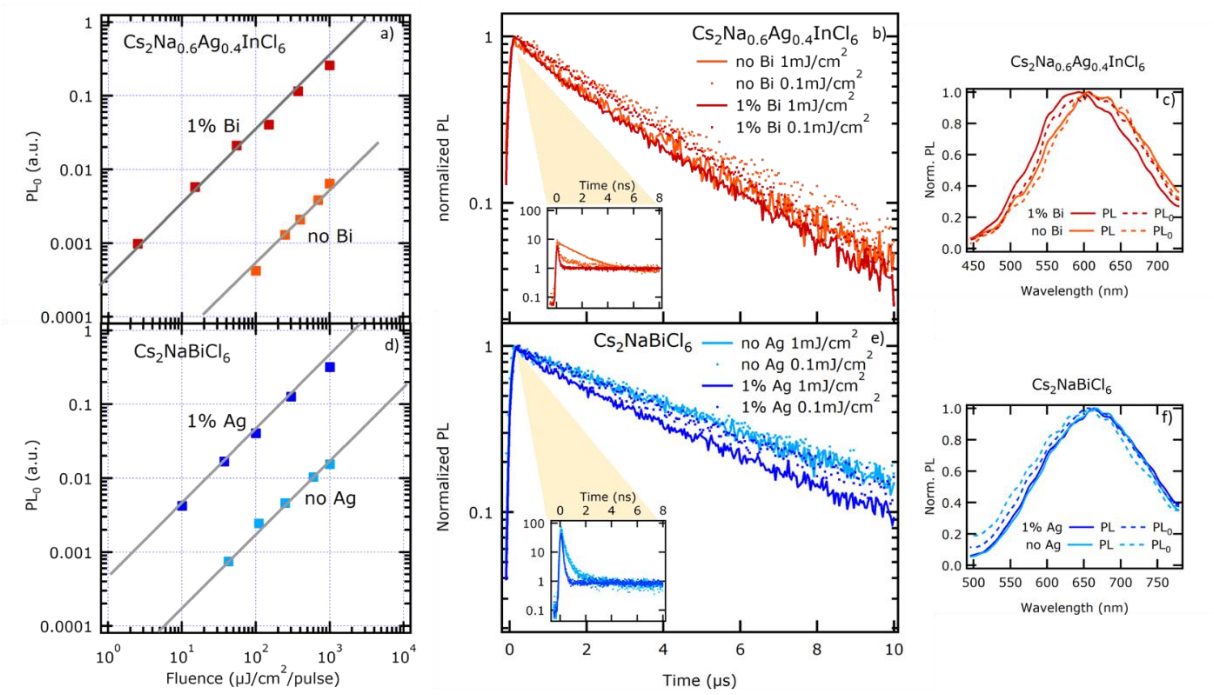

Fig. S8 Study of PL linearity for two reference composites: upper part are reported $Cs_2Na_{0.6}Ag_{0.4}InCl_6$ with (red) and without (orange) 1% Bi doping, lower part $Cs_2NaBiCl_6$ with (blue) and without (light blue) 1% Ag doping. Squares in plots a) and b) are PL intensity at zero time delay (PL_0), as extracted from TRPL measurements with sub-ns time resolution, as a function of excitation fluence, to be compared with grey lines representing slope 1. The linearity study is supported also by the decay profiles of TRPL at different excitation fluences b) e), with their behavior at short timescales shown in the insets. PL emission spectra reported in c) and f) are not modified by doping and are the same for long-delay (solid lines) and at zero time delay (dashed lines), ensuring us that they are coming from the same STE emitting species. Both the long- and short-timescale decay features reported in b) and e) are not noticeably affected by power or by Ag/Bi doping. These results are all confirming that our measurements are performed in linearity regime.

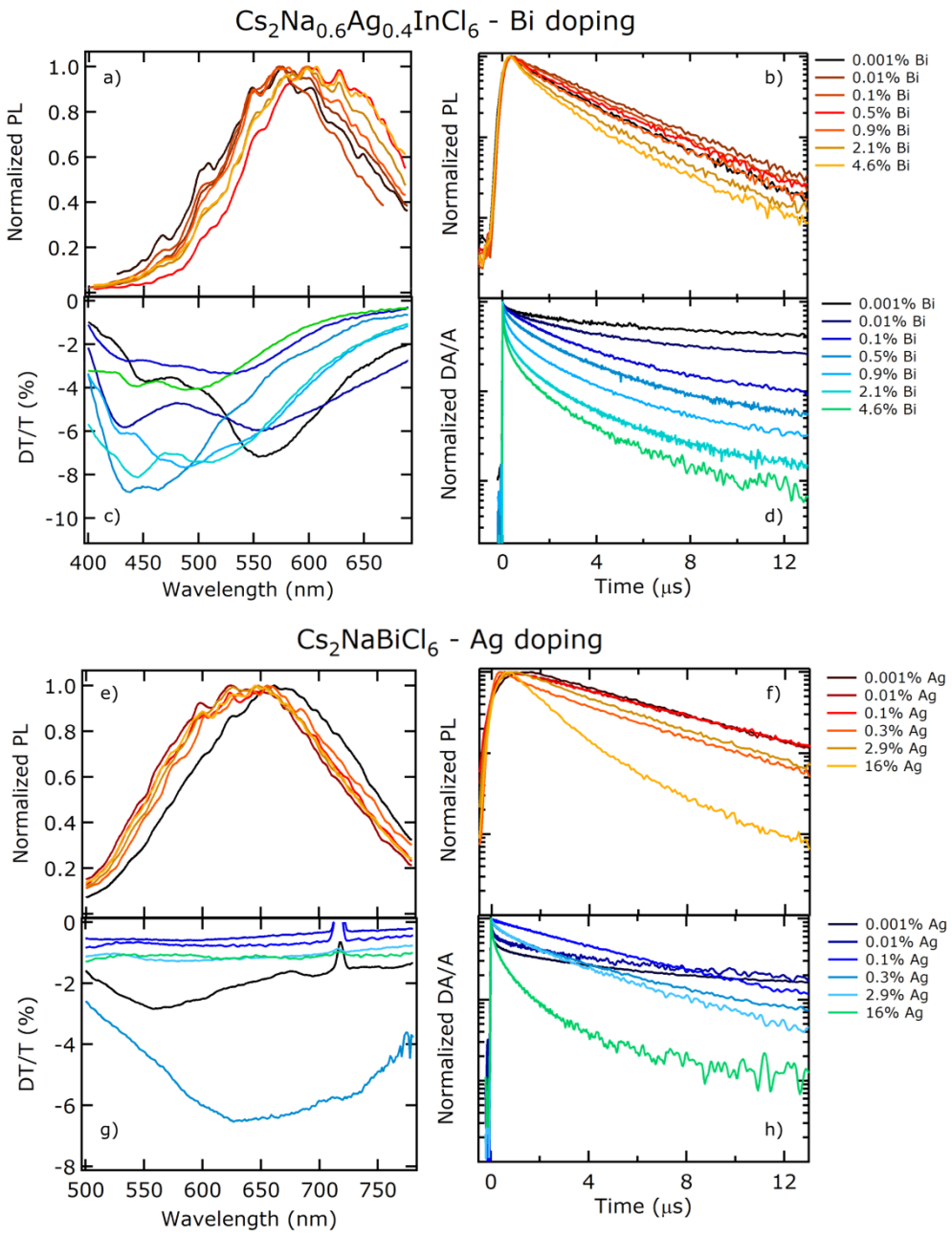

Fig. S9 Comparative series of normalized PL spectra (left) and decay profiles (right) for $Cs_2Na_{0.6}Ag_{0.4}InCl_6$ when Bi is partially substituted, a)-d), and $Cs_2NaBiCl_6$ with partial Ag substitution, e)-h). Photoinduced absorption signals, appearing as negative DT/T spectra (d and e), were converted to DA/A for an easier visualization of the decay profiles (d and h). Measurements are performed in tandem TA/TRPL configuration, taken with same excitation condition, with an excitation fluence of 1 mJ/cm^2/pulse.

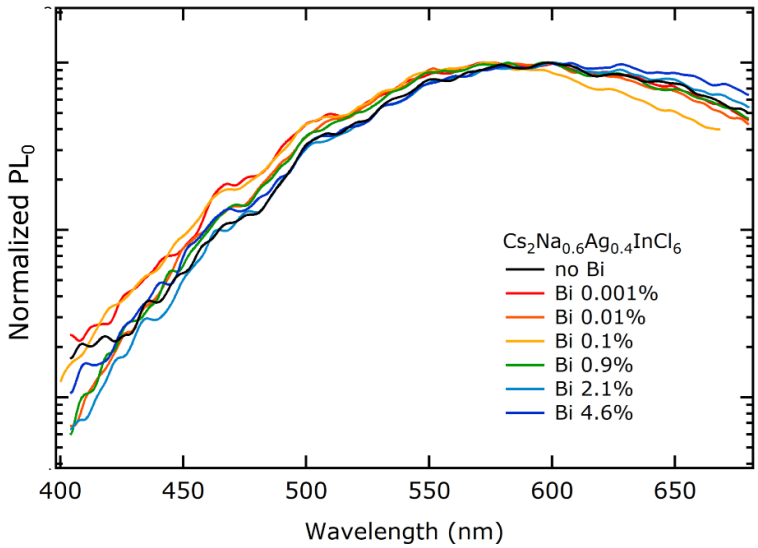

Fig. S10 Results of TRPL measurements on $Cs_2Na_{1-x}Ag_xInCl_6$ crystals with various amounts of Bi inclusion. The PL spectra are normalized to peak and are taken in a spectral window of 100 ps around the arrival of the excitation pulse.